Identification of MYC as an antinecroptotic protein that stifles RIPK1–RIPK3 complex formation

Daehyeon Seong[a,1], Manhyung Jeong[a,1], Jinho Seo[a,b], Ji-Yoon Lee[c], Chi Hyun Hwang[a], Ho-Chul Shin[d], Jeong Yoon Shin[a], Young Woo Nam[a], Jeong Yeon Jo[e], Haeseung Lee[f], Hye-Jung Kim[g], Hwa-Ryeon Kim[a], Ji Hoon Oh[a], Sang-Jun Ha[a], Seung Jun Kim[d], Jae-Seok Roe[a], Wankyu Kim[f], June-Won Cheong[h], Kwang-Hee Bae[c], Sang Chul Lee[c], Andrew Oberst[i], Peter Vandenabeele[j,k], Dong Hoon Shin[e], Eun-Woo Lee[c,2], and Jaewhan Song[a,2]

[a]Department of Biochemistry, College of Life Science and Biotechnology, Yonsei University, 120-749 Seoul, Republic of Korea; [b]Environmental Diseases Research Center, Korea Research Institute of Bioscience and Biotechnology, 34141 Daejeon, Republic of Korea; [c]Metabolic Regulation Research Center, Korea Research Institute of Bioscience and Biotechnology, 34141 Daejeon, Republic of Korea; [d]Disease Target Structure Research Center, Korea Research Institute of Bioscience and Biotechnology, 34141 Daejeon, Republic of Korea; [e]Research Institute, Department of Cancer Biomedical Science, Graduate School of Cancer Science and Policy, National Cancer Center, 10408 Goyang, Republic of Korea; [f]Department of Life Sciences, Ewha Research Center for Systems Biology, Ewha Womans University, 03760 Seoul, Republic of Korea; [g]New Drug Development Center, Korea Biotechnology Industry Organization Osong Medical Innovation Foundation, 28160 Cheongju-si, Republic of Korea; [h]Division of Hematology, Department of Internal Medicine, Severance Hospital, Yonsei University College of Medicine, 03722 Seoul, Republic of Korea; [i]Department of Immunology, University of Washington, Seattle, WA 98109; [j]Vlaams Instituut voor Biotechnologie-University of Ghent Center for Inflammation Research, Vlaams Instituut voor Biotechnolgie, 9052 Ghent, Belgium; and [k]Department of Biomedical Molecular Biology, Ghent University, 9000 Ghent, Belgium

Edited by John Silke, The Walter and Eliza Hall Institute, Parkville, VIC, Australia, and accepted by Editorial Board Member Anton Berns July 6, 2020 (received for review January 23, 2020)

The underlying mechanism of necroptosis in relation to cancer is still unclear. Here, MYC, a potent oncogene, is an antinecroptotic factor that directly suppresses the formation of the RIPK1–RIPK3 complex. Gene set enrichment analyses reveal that the MYC pathway is the most prominently down-regulated signaling pathway during necroptosis. Depletion or deletion of MYC promotes the RIPK1–RIPK3 interaction, thereby stabilizing the RIPK1 and RIPK3 proteins and facilitating necroptosis. Interestingly, MYC binds to RIPK3 in the cytoplasm and inhibits the interaction between RIPK1 and RIPK3 in vitro. Furthermore, MYC-nick, a truncated form that is mainly localized in the cytoplasm, prevented TNF-induced necroptosis. Finally, down-regulation of MYC enhances necroptosis in leukemia cells and suppresses tumor growth in a xenograft model upon treatment with birinapant and emricasan. MYC-mediated suppression of necroptosis is a mechanism of necroptosis resistance in cancer, and approaches targeting MYC to induce necroptosis represent an attractive therapeutic strategy for cancer.

MYC | RIPK3 | TNF-α | necroptosis

Necroptosis is a programmed cell death pathway that is executed by the necrosome complex, which comprises receptor-interacting protein kinases such as RIPK1 and RIPK3 (1–4). The binding of TNF-α to TNF receptor 1 induces the activation of RIPK3, which phosphorylates downstream mixed lineage kinase domain-like protein (MLKL) (5–7). Phosphorylated MLKL forms an oligomer and functions as a necroptosis executioner by directly or indirectly disrupting plasma membrane integrity (8–12). While the molecular mechanisms and physiological relevance of necroptosis have been relatively well studied, little is known about the contributions of necroptosis to tumorigenesis and tumor progression (13–19).

Numerous studies have focused on the effect of necroptosis on cancer treatment (20). Various anticancer agents, such as death receptor ligands (TNF-α and TRAIL [tumor necrosis factor-related apoptosis-inducing ligand]), caspase inhibitors (zVAD-fmk and IDN-6556), Smac mimetics, staurosporine, 5-fluorouracil, cisplatin, and FTY720, have been reported to induce necroptotic cell death in cancer cells, although the precise mechanisms and target molecules involved in the execution of necroptosis require further examination (21, 22). However, cancer cells also possess or can develop strategies to escape necroptosis and apoptosis to survive under necroptosis-inducing conditions (23–25). Therefore, elucidation of the interplay between necroptosis and cancer cells would provide insights into necroptosis-targeted cancer treatment.

The transcription factor MYC is a representative oncoprotein that regulates various cellular processes, including cell proliferation, differentiation, inflammation, and metabolism (26–28). Here, we demonstrate that MYC functions as an antinecroptotic factor by inhibiting the RIPK1 and RIPK3 interaction, indicating that cancer cells may use MYC overexpression as a strategy to escape necroptotic cell death. These observations highlight the dynamic interplay between necroptosis and the oncoprotein MYC, suggesting a prospective therapeutic strategy.

Significance

A major yet perplexing question in the field of necroptosis is the role and involvement of necroptosis in cancer cells. Many cancer cells have protective mechanisms against necroptosis, but the underlying mechanism remains elusive. We report findings of cross-talk and a regulatory pathway that exist between MYC, a potent oncogene, and RIPK3, a pivotal factor in necroptosis. We find that MYC pathway is downregulated upon necroptotic, while MYC inhibits TNF-α–induced necroptosis. The inhibitory effect of MYC on necroptosis is unexpected because no transcriptional activity by MYC is required. Mechanistically, a direct interaction between MYC and RIPK3 takes place in the cytosol, preventing RIPK1–RIPK3 complex formation. Finally, MYC depletion enhances antitumor activity of necroptosis-inducing agents in a xenograft model.

Author contributions: D.S., M.J., E.-W.L., and J. Song designed research; D.S., M.J., J. Seo, J.-Y.L., C.H.H., J.Y.S., Y.W.N., J.Y.J., H.L., H.-J.K., H.-R.K., J.H.O., D.H.S., and E.-W.L. performed research; J.-W.C. contributed new reagents/analytic tools; D.S., M.J., J. Seo, H.-C.S., S.-J.H., S.J.K., J.-S.R., W.K., J.-W.C., K.-H.B., S.C.L., A.O., P.V., E.-W.L., and J. Song analyzed data; and D.S., M.J., E.-W.L., and J. Song wrote the paper.

The authors declare no competing interest.

This article is a PNAS Direct Submission. J.S. is a guest editor invited by the Editorial Board.

[1]D.S. and M.J. contributed equally to this work.

[2]To whom correspondence may be addressed. Email: ewlee@kribb.re.kr or jso678@yonsei.ac.kr.

This article contains supporting information online at https://www.pnas.org/lookup/suppl/doi:10.1073/pnas.2000979117/-/DCSupplemental.

First published August 4, 2020.

Results

TNF-α–Dependent Necroptosis Induces MYC Down-Regulation. We first searched for the pathways that are affected by necroptosis by performing an RNA-sequencing analysis of HT-29 human colon cancer cells followed by a gene set enrichment analysis (GSEA) to identify new signaling pathways associated with necroptosis. For these analyses, HT-29 cells were treated with TNF-α, the cIAP inhibitor BV6, and the pan-caspase inhibitor zVAD-fmk (TBZ) for 4 h to induce necroptosis, as previously reported (2, 29, 30). MLKL-depleted HT-29 cells were also used to prevent necroptotic cell death and monitor the long-term effects of necroptosis (5). Consistent with previous studies, target gene sets of inflammatory transcription factors were enriched in HT-29 cells treated with TBZ compared to the cells administered the control treatment (*SI Appendix*, Fig. S1 *A* and *B*) (31–33). Interestingly, target gene sets for MYC/MAX were significantly down-regulated in cells treated for 4 h and 12 h (*SI Appendix*, Fig. S1 *A* and *B*). Necroptotic cell gene signatures showed inverse correlations with various MYC-related gene sets (*SI Appendix*, Fig. S1*C*). These changes were also observed in MLKL-depleted cells subjected to necroptotic stress for 5 h, further suggesting that necroptosis signaling might induce downstream changes in MYC transcription independent of MLKL-mediated necroptotic cell death (*SI Appendix*, Fig. S1 *D* and *E*). When the GSEA data were further confirmed by directly measuring the levels of various proteins in cells under necroptotic stimulation, the levels of inflammatory signaling markers, including IKK, p100/p52 (noncanonical NF-κB), JNK, c-Fos, and c-Jun, were consistently increased (*SI Appendix*, Fig. S1*F*). Strikingly, among the oncogenes detected, only the MYC protein rapidly vanished during the necroptotic process (*SI Appendix*, Fig. S1*F*). Accordingly, mRNA levels of several MYC target genes are indeed altered during necroptosis, suggesting that MYC might be associated with the necroptosis signaling pathway (*SI Appendix*, Fig. S1*G*).

RIPK3 Activation Leads to the Proteasomal Degradation of MYC during Necroptosis. We next evaluated whether MYC expression was also affected by canonical TNF-α signaling. However, the MYC levels were slightly increased in cells stimulated with TNF-α alone or TNF-α plus BV6 (TB), which led to NF-κB activation, as evidenced by cIAP2 induction, or apoptosis, as evidenced by poly(ADP-ribose) polymerase (PARP) cleavage (*SI Appendix*, Fig. S2*A*). The inhibition of caspase activity with zVAD-fmk, which leads to RIPK3 phosphorylation, down-regulated MYC, suggesting that MYC suppression might occur downstream of complex IIb formation and might require RIPK3 activation (*SI Appendix*, Fig. S2 *A* and *B*) (34). Furthermore, treatment of the FADD-deficient (FADD-def.) Jurkat cells with TNF-α alone or TNF-α plus birinapant, which is known to induce necroptosis (35), reduced the levels of the MYC protein (*SI Appendix*, Fig. S2*C*) (35). Consistently, the treatment of HeLa cells stably expressing RIPK3 with TNF-α, BV6, and zVAD-fmk decreased MYC expression, which was not observed in HeLa cells lacking RIPK3 expression, indicating that RIPK3 is required for MYC down-regulation (*SI Appendix*, Fig. S2*D*). Similarly, MYC up-regulation induced by TNF-α alone and down-regulation by necroptotic stimulation were also observed in L929 murine fibroblasts and TC-1 murine lung cancer cells, indicating a conserved mechanism underlying necroptosis-mediated MYC down-regulation (*SI Appendix*, Fig. S2 *E* and *F*). Since necroptotic cells release DAMP molecules that influence neighboring cells (33), we tested whether MYC down-regulation is mediated by paracrine signaling. However, the conditioned medium from necroptotic cells did not affect MYC expression, suggesting that necroptosis induces MYC down-regulation in a cell-autonomous manner (*SI Appendix*, Fig. S2*G*)

To identify the plausible pathways involved in MYC down-regulation, we employed several inhibitors of necroptosis signaling proteins, such as RIPK1, RIPK3, and MLKL. Notably, down-regulation of MYC during necroptosis was prevented by two RIPK1 inhibitors (necrostatin-1 [Nec-1] and GSK′963) and a RIPK3 inhibitor (GSK′872), but not by the MLKL inhibitor (necrosulfonamide [NSA]) (*SI Appendix*, Fig. S2 *H* and *I*). In addition, RIPK3 depletion prevented MYC down-regulation, whereas the levels of the MYC protein were decreased in MLKL-depleted cells (*SI Appendix*, Fig. S2 *J* and *K*). Based on these data, RIPK3 activation induces MYC down-regulation during necroptosis in an MLKL-independent manner.

We next investigated how MYC is down-regulated upon necroptosis. When levels of the MYC mRNA were assessed using qRT-PCR, levels of the MYC mRNA decreased at 1 h post-TBZ stimulation but recovered after 3 to 5 h (*SI Appendix*, Fig. S2*L*). An early decrease in the mRNA levels of MYC was also observed when cells were treated with TNF-α alone or TB, suggesting that the down-regulation of the MYC mRNA after 1 h of stimulation was not specific to necroptosis (*SI Appendix*, Fig. S2*L*). In addition, the MYC mRNA levels rebounded upon necroptosis, whereas the levels of the MYC protein were still decreased, suggesting that the levels of the MYC protein are regulated posttranslationally (*SI Appendix*, Fig. S2 *A* and *M*).

To address whether MYC is degraded by the proteasome upon necroptosis, we stimulated HT-29 cells with TBZ in the presence of MG132, a proteasome inhibitor. However, proteasome inhibition completely abrogated the activation of the RIPK3 pathway, as previously reported (36), in part by suppressing the cIAP1 degradation induced by BV6, resulting in sustained MYC expression (*SI Appendix*, Fig. S2*N*). Thus, MG132 was added after a 2-h stimulation of HT-29 cells with TBZ, enabling early RIPK3 activation, and MYC destabilization was prevented by MG132 (*SI Appendix*, Fig. S2*O*). The observation that ectopically introduced MYC was also degraded during necroptosis excludes the possibility of transcriptional control of MYC by necroptosis (*SI Appendix*, Fig. S2*P*). Finally, we observed an increase in the polyubiquitination of endogenous MYC during necroptosis (*SI Appendix*, Fig. S2*Q*). Collectively, these data indicate that necroptosis induces the polyubiquitination and proteasomal degradation of MYC.

MYC Functions as an Antinecroptotic Factor in TNF-α–Induced Necroptosis. Although MYC is known to play key roles in cell proliferation and apoptosis (37, 38), its role in necroptosis is unknown. The decreased levels of MYC upon necroptotic stimulation prompted us to search for a possible role for MYC in necroptosis. When MYC was ablated using small-interfering RNA (siRNA) pools containing four different siRNAs against MYC, HT-29 cells became exceptionally susceptible to TBZ-induced cell death and showed increased levels of phospho-RIPK3 and phospho-MLKL (Fig. 1 *A*–*C*). However, HT-29 cells stably expressing MYC became resistant to necroptosis and showed delays in the phosphorylation of RIPK3 and MLKL (Fig. 1 *D*–*F*). Notably, in cells with varying degrees of MYC overexpression, the cell death process was increasingly inhibited in proportion to the increasing concentration of MYC, indicating the compelling anti-necroptotic effects of MYC at different concentrations (Fig. 1 *G* and *H*). Reconstitution of siRNA-resistant MYC ($MYC^{Res\#1}$) in MYC-depleted cells reversed the sensitivity to necroptosis and the RIPK3 and MLKL phosphorylation, suggesting that MYC is a negative regulator of necroptosis (Fig. 1 *I* and *J*).

We generated two MYC knockout (KO) cell lines, KO#1 and #2 using the CRISPR/Cas9 method and confirmed MYC KO by sequencing and immunoblot analyses to further validate the negative effect of MYC on necroptosis and eliminate any off-target effects (*SI Appendix*, Fig. S3 *A*–*C*). Consistent with the results of the knockdown experiments, both of the MYC KO cell lines were more sensitive to TBZ-induced necroptosis than

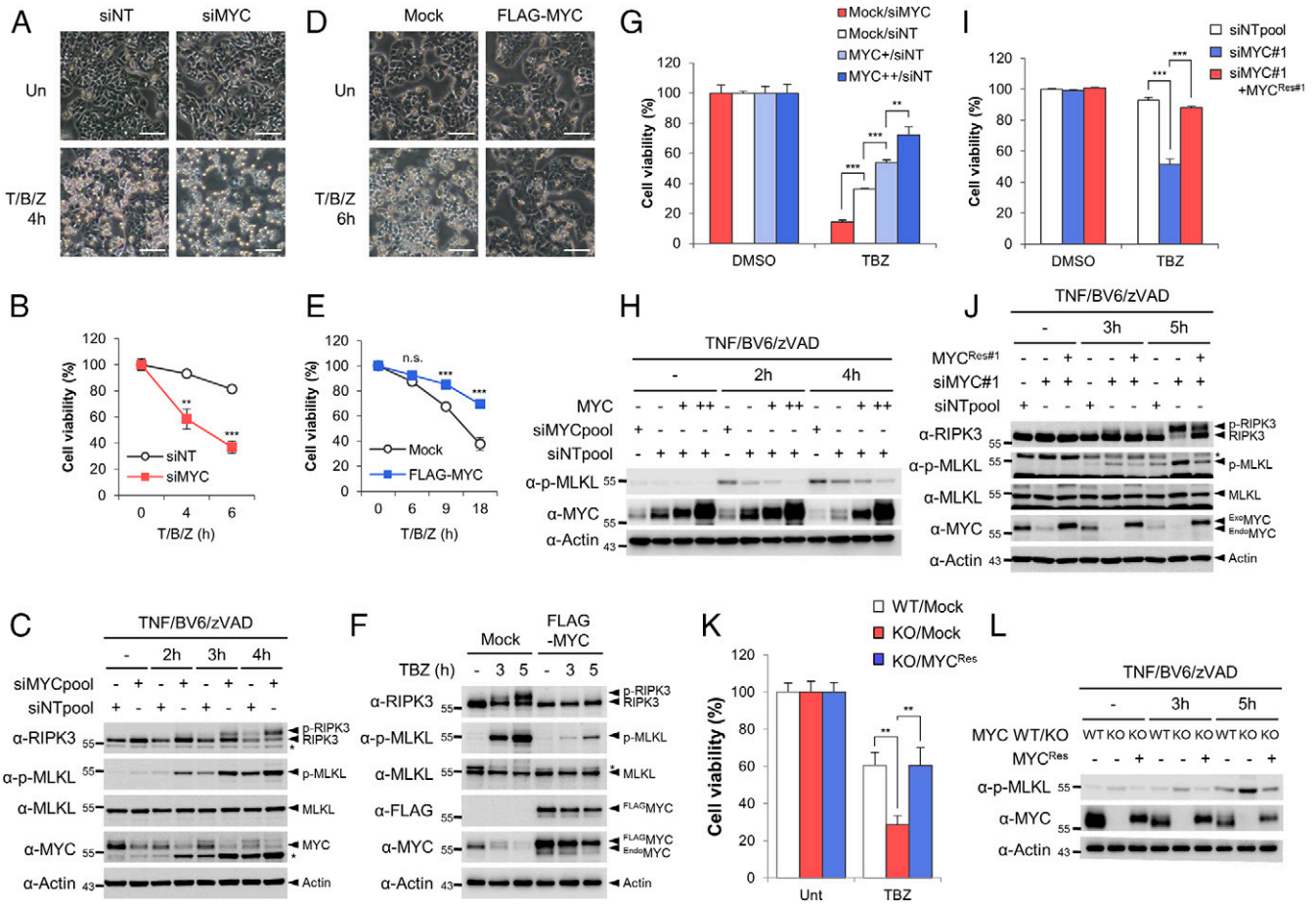

Fig. 1. MYC suppresses TBZ-induced necroptosis. (*A–C*) MYC depletion facilitates necroptosis. HT-29 cells transfected with a nontargeting siRNA pool (siNT) or MYC siRNA pool (siMYC) were treated with TBZ as indicated and subjected to a photomicrograph analysis (*A*), cell viability analysis (*B*), and immunoblotting analysis (*C*). Data are the means ± SD, $n = 3$, with $^{**}P < 0.01$ and $^{***}P < 0.001$ compared to siNT with a two-sided Student's *t* test. (Scale bars, 100 μm.) The asterisk in *C* indicates MLKL or p-MLKL. (*D–F*) MYC overexpression delays necroptosis. HT-29 cells stably expressing Mock or MYC were treated with TBZ for the indicated times and analyzed as described in *A–C*. Data are the means ± SD, $n = 3$, with $^{***}P < 0.001$ and n.s. = nonsignificant compared to the mock control with two-sided Student's *t* test. (Scale bars, 100 μm.) (*G* and *H*) MYC suppresses necroptosis in a dose-dependent manner. HT-29 cells were transduced with increasing amounts of lentiviral MYC or the mock control. Stable HT-29 cell lines were transfected with siNT or siMYC as indicated and treated with TBZ for 18 h for assessments of cell viability (*G*) or for 2 to 4 h for the immunoblot analysis (*H*). (*I* and *J*) MYC reconstitution rescues MYC-depleted HT-29 cells from accelerated necroptosis. HT-29 cells stably expressing siRNA-resistant MYC ($MYC^{Res\#1}$) were transfected with individual MYC siRNA (siMYC#1) and treated with TBZ for 6 h (*I*) or the indicated times (*J*). After TBZ stimulation, HT-29 cells were analyzed as described in (*B* and *C*). The asterisk indicates RIPK3. (*K* and *L*) CRISPR/Cas9-mediated KO of MYC enhances necroptosis, which is rescued by MYC^{Res} overexpression. MYC KO#1 HT-29 cells lentivirally transduced with Mock or MYC^{Res} were treated with TBZ for 10 h (*K*) or the indicated times (*L*). Data are the means ± SD, $n = 3$, with $^{**}P < 0.01$ according to a two-sided Student's *t* test.

TB-induced apoptosis (*SI Appendix*, Fig. S3 *D* and *E*). Reconstitution of MYC expression (MYC^{Res}) in the MYC KO#1 cell line again reversed the sensitivity to necroptosis (Fig. 1 *K* and *L*).

We next asked whether MYC depletion might affect other necroptotic signaling pathways. TNF-α–induced necroptosis sensitized by CHX or 5z7 (TAK1 inhibitor) was further increased by MYC depletion in HT-29 cells (*SI Appendix*, Fig. S4*A*). In addition, necroptosis induced by TNF-α alone (T), TNF-α/birinapant (T/Bir), or TNFα/5z7 (T/5z) in FADD-def. Jurkat cells was also enhanced following MYC depletion (*SI Appendix*, Fig. S4*B*). Furthermore, MYC-depleted cells were more sensitive to necroptosis induced by other stimuli—such as TRAIL, LPS, and IFN-γ—all of which depend on RIPK3 (*SI Appendix*, Fig. S4 *C–E*). Consistent with the results obtained from human cells, mouse L929 and TC-1 cells showed increased sensitivity to TZ- or TBZ-induced necroptosis upon MYC depletion (*SI Appendix*, Fig. S4 *F–I*). These data suggest a conserved role for MYC in regulating TNF-α–induced necroptosis.

We next examined whether MYC also affects the RIPK1-dependent apoptosis induced by TNF-α plus Smac mimetics. MYC ablation failed to promote TNF-α–mediated apoptosis, but it facilitated the necroptosis of HT-29 and HeLa-RIPK3 cells (Fig. 2 *A–D*). The increase in necroptosis induced by MYC depletion was prevented by Nec-1, indicating the association of MYC with necroptosis (Fig. 2 *A–D*). MYC depletion increased the levels of the phosphorylated forms of RIPK3 and MLKL, as well as MLKL oligomerization (Fig. 2 *C* and *E*), suggesting that MYC might be involved in the pivotal regulatory axis of the RIPKs and MLKL.

MYC Suppresses TNF-α–Induced Necroptosis by Suppressing Necrosome Formation. Since the formation of complex IIb and the necrosome are essential for apoptosis and necroptosis, we examined the effect of MYC on the formation of these complexes upon stimulation (34). The TBZ-induced recruitment of necrosome components, such as RIPK3, RIPK1, MLKL, and FADD to caspase-8 was increased in the MYC-depleted and MYC-KO cells compared to the control cells (Fig. 3 *A* and *B*). However, remarkable increases in TB-induced complex IIb formation were not observed in HT-29

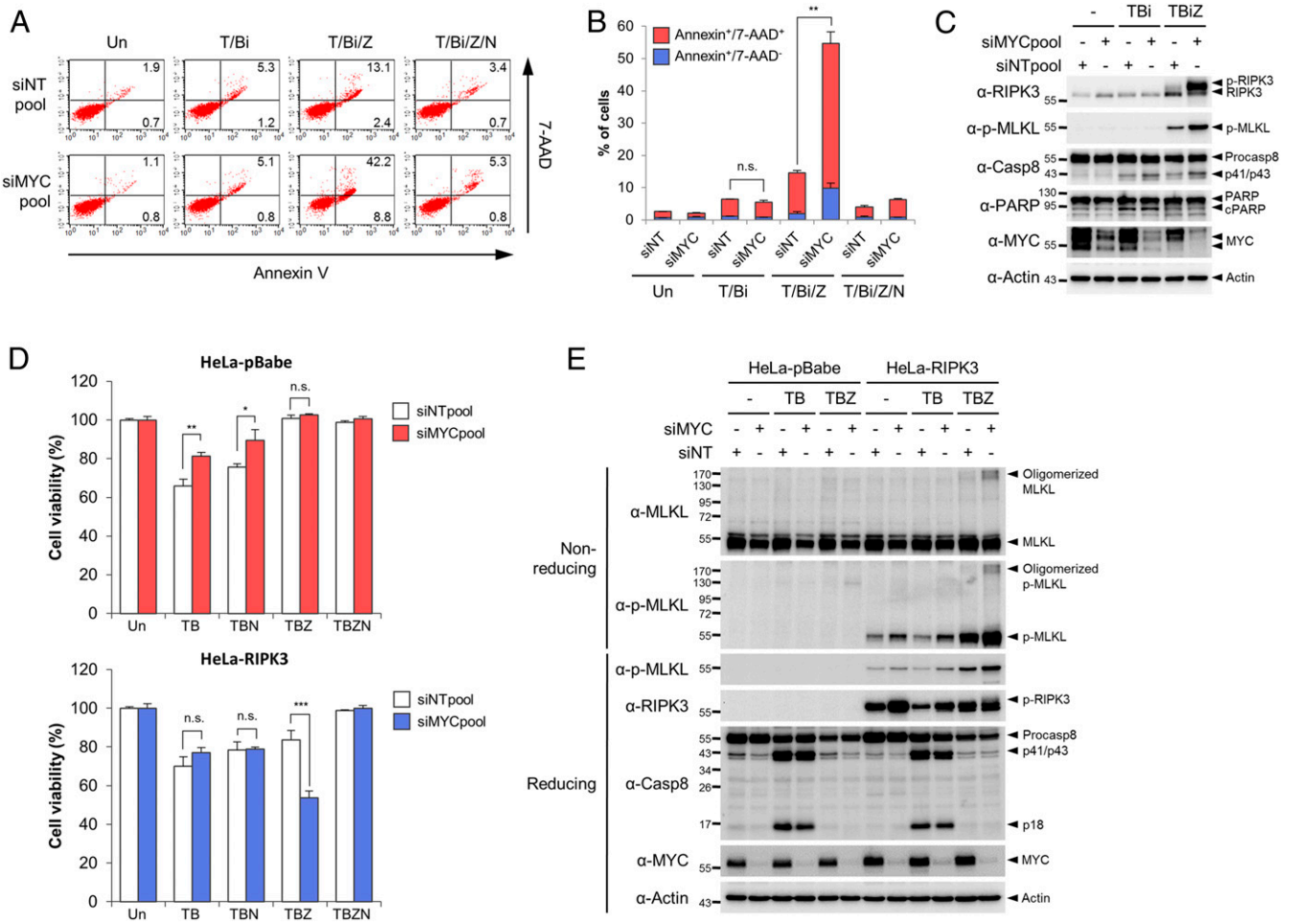

Fig. 2. MYC restrains necroptosis but not apoptosis. (*A* and *B*) MYC knockdown facilitates necroptosis but not apoptosis. HT-29 cells transfected with siNT or siMYC were treated with T/Bi, T/Bi/Z, or T/Bi/Z plus Nec-1 (T/Bi/Z/N) for 6 h. After 6 h, the cells were stained with Annexin V and 7-AAD for flow cytometry analysis. A representative plot is shown in *A*, and three independent analyses are shown in *B*. Data are the mean s± SD, $n = 3$, with $^{**}P < 0.01$ and n.s. = nonsignificant compared to siNT with a two-sided Student's *t* test. (*C*) HT-29 cells transfected with siNT or siMYC were treated with TBi or TBiZ. Activation of the necroptosis or apoptosis pathways was analyzed by evaluating the phosphorylation of RIPK3 and MLKL and cleavage of caspase-8 and PARP using immunoblotting. (*D*) MYC depletion accelerates TBZ-induced necroptosis, but not TB-induced apoptosis, in HeLa-RIPK3 cells. The HeLa stable cell line constitutively expressing mock (HeLa-pBabe) or RIPK3 (HeLa-RIPK3) was treated with TB for 6 h or TBZ for 4 h and examined for cell viability. Data are the means ± SD, $n = 3$, with $^{*}P < 0.05$, $^{**}P < 0.01$, $^{***}P < 0.001$ and n.s. = nonsignificant compared to siNT with a two-sided Student's *t* test. (*E*) The HeLa cells constitutively expressing the mock (HeLa-pBabe) or RIPK3 plasmid (HeLa-RIPK3) were treated with TB for 3 h or TBZ for 2 h and lysed in nonreducing buffer or reducing buffer containing β-mercaptoethanol, followed by immunoblot analyses.

cells or HeLa cells upon MYC depletion, both of which lack RIPK3 activation (Fig. 3 *A* and *C*). To further validate necrosome formation, we carried out gel-filtration analysis. Similar to previous observations, upon TBZ stimulation, the RIPK1, RIPK3, and MLKL proteins were detected in a greater than 2-MDa fraction, which might be the necrosome (Fig. 3*D*) (29, 39, 40). Although most of these proteins were still present in their monomeric forms in control cells treated with TBZ, large portions of RIPK3, RIPK1, and MLKL shifted to earlier 2-MDa fractions in the MYC-depleted cells treated with TBZ, suggesting that MYC constrains necrosome formation (Fig. 3*D*). Although MYC negatively regulates necrosome formation, this molecule was not detected in complex IIb or in the necrosome (Fig. 3*A*). Furthermore, little change was observed in the fraction containing the MYC proteins in the gel-filtration analyses upon necroptotic stimulation, suggesting that MYC might not be an integral part of the necrosome complexes (Fig. 3*D*).

Cytoplasmic MYC Functionally Suppresses RIPK3-Dependent Necroptosis. Because MYC is a transcription factor (41), we aimed to determine whether MYC transcriptional activity is involved in the suppression of necroptosis. When MAX, a cofactor of MYC (42), was depleted in HT-29 cells, cell viability and the levels of necroptotic markers, such as p-MLKL and p-RIPK3, were relatively unchanged, suggesting that MAX might not be involved in this process (Fig. 4 *A*–*D*). Since MYC is also localized to the cytoplasm (Fig. 4*E*) (43–45) and appears to regulate the necrosome complex, we asked whether cytoplasmic MYC might suppress necroptosis. We constructed a series of MYC mutants with point mutations in nuclear localization signals (NLSs) 1 and 2 to address these questions; these point mutants show weak localization or lack the ability to localize to the nucleus based on previous reports (41). Among the various MYC mutants, the NLS1/2 mutant—with lysine residues at 323, 326, and 371 and arginine residues at 364, 366, and 367 replaced with alanine residues—was almost completely excluded from the nucleus and was defective in inducing its target-gene expression (*SI Appendix*, Fig. S5 *A*–*D*). This mutant still suppressed necroptosis as well as MYC WT, indicating that cytoplasmic MYC might suppress TNF-α–induced necroptosis (*SI Appendix*, Fig. S5*E*). Furthermore, the

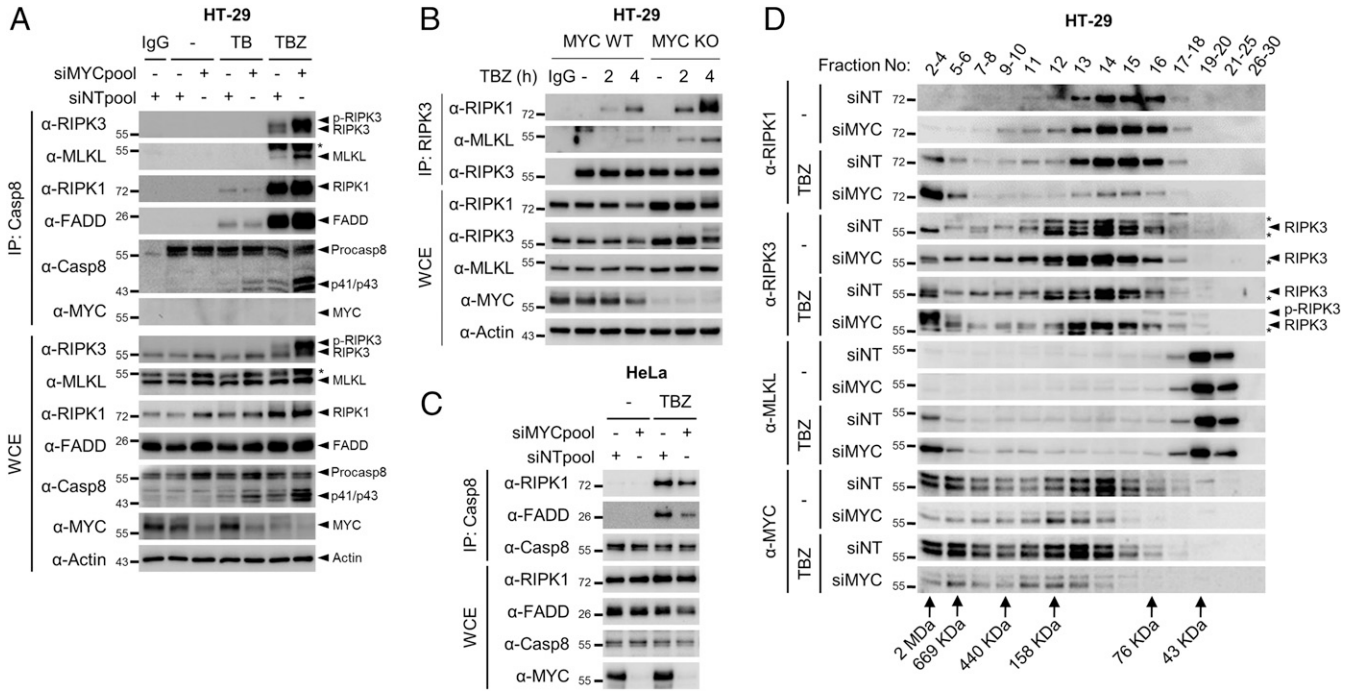

Fig. 3. MYC negatively regulates the formation of the RIPK3-containing necrosome. (*A*) MYC depletion promotes necrosome formation upon TBZ stimulation. HT-29 cells transfected with siNT or siMYC were treated with TB or TBZ. After treatment, the cell lysates were immunoprecipitated with an anticaspase-8 antibody and analyzed using immunoblotting. The asterisk indicates RIPK3. (*B*) MYC deletion facilitates necrosome formation. MYC WT and KO HT-29 cells were treated with TBZ for the indicated times, followed by immunoprecipitation with an RIPK3 antibody. (*C*) MYC depletion does not regulate TBZ-induced RIPK1-dependent complex IIb formation in HeLa cells. HeLa cells were transfected with siMYC and treated with TBZ for 3 h. The complex IIb was isolated by immunoprecipitation of caspase-8. (*D*) HT-29 cells were transfected with the indicated siRNA and treated with TBZ for 3 h. The cell lysates were fractionated according to molecular size by gel-filtration chromatography and examined using immunoblotting.

NLS1/2 mutant restored the increased necroptotic cell death after the MYC deletion (Fig. 4 *F* and *G*).

We employed a cleaved fragment of endogenous MYC named MYC-nick that does not contain the NLSs and is known to localize exclusively in the cytoplasm with no MYC transcriptional activities to further determine if the cytosolic function of MYC is physiologically associated with the suppression of necroptosis (46, 47). We also detected two cytoplasmic isoforms of MYC with molecular masses of ∼40 kDa and 50 kDa in HT-29 cells cultured at high density, as previously reported (Fig. 5*A*) (46, 47). Although MYC-nick is reported to be a 42-kDa protein (46, 47), FLAG-MYC-nick (1–298) is detected at ∼55 kDa (Fig. 5*B*). Furthermore, this band was not detected in cells expressing the Δ290–300 mutant of MYC, which is resistant to protease cleavage and does not produce MYC-nick (Fig. 5*C*) (46, 47). Therefore, we concluded that the band detected at ∼50 kDa is an endogenous MYC-nick (1–298) isoform in HT-29 cells under our conditions, and size difference of MYC-nick compared to other reports might be derived from difference in Western blotting protocol and molecular weight markers. The levels of MYC-nick were also decreased relative to MYC WT in cells exposed to necroptotic stimuli (Fig. 5*D*). The reduction in MYC-nick levels might be due to the reduced levels of MYC and the degradation of MYC-nick itself during necroptosis, since the levels of ectopic MYC-nick were also decreased following necroptosis (*SI Appendix*, Fig. S6*A*). Notably, MYC-nick suppressed MLKL phosphorylation and necroptotic cell death (Fig. 5*E* and *SI Appendix*, Fig. S6).

Since the cytoplasmic NLS1/2 mutant and MYC-nick could inhibit necroptosis, we hypothesized that MYC would interact with RIPK3 in the cytoplasm. First, MYC was observed to directly interact with RIPK3 in vivo and in vitro (*SI Appendix*, Fig. S7 *A* and *B*). Physiologically, endogenous MYC was associated with endogenous RIPK3, and this association was abolished upon necroptosis (*SI Appendix*, Fig. S7 *C* and *D*). The dissociation of MYC from RIPK3 was abrogated by GSK′963, but not by GSK′872, suggesting that RIPK1 kinase activity, but not RIPK3 kinase activity, is responsible for the dissociation (*SI Appendix*, Fig. S7*D*). In particular, MYC and RIPK3 were colocalized and interacted in the cytoplasm (Fig. 5 *F* and *G* and *SI Appendix*, Fig. S7*E*). Furthermore, both full-length MYC and MYC-nick also interacted with RIPK3 in the cytoplasm, supporting our observation that both MYC and MYC-nick would participate in suppressing necroptosis in the cytoplasm (Fig. 5 *H* and *I*). Notably, endogenous MYC-nick, similar to MYC, interacted with RIPK3 in HT-29 cells (Fig. 5*J*). Indeed, the Δ290–300 mutant defective in MYC-nick production still prevented necroptosis (Fig. 5 *C* and *K*). Based on these data, both cytoplasmic MYC WT and MYC-nick might be responsible for preventing necroptosis in HT-29 cells. In addition to RIPK3, RIPK1 also interacted with MYC (*SI Appendix*, Fig. S7 *F* and *G*). However, we failed to detect the endogenous interaction between MYC and RIPK1, possibly suggesting a very transient or weak interaction between the two proteins (*SI Appendix*, Fig. S7 *H* and *I*).

MYC Prevents the Formation of RIPK1–RIPK3 Complexes, Suppressing Necroptosis. Since MYC directly binds to RIPK3 and inhibits RIPK3 activation, we hypothesized that MYC might directly hinder the complex formation between RIPK3 and RIPK1. Interestingly, the interaction between RIPK1 and RIPK3 was reduced upon MYC overexpression, indicating that necrosome formation was decreased in HT-29 cells stably expressing MYC (Fig. 6*A*). Furthermore, the increased necrosome formation observed in MYC KO cells during necroptosis was suppressed by the reconstitution with MYC WT or the NLS1/2 mutant (*SI Appendix*, Fig. S5*F*). Notably, recombinant GST-MYC purified

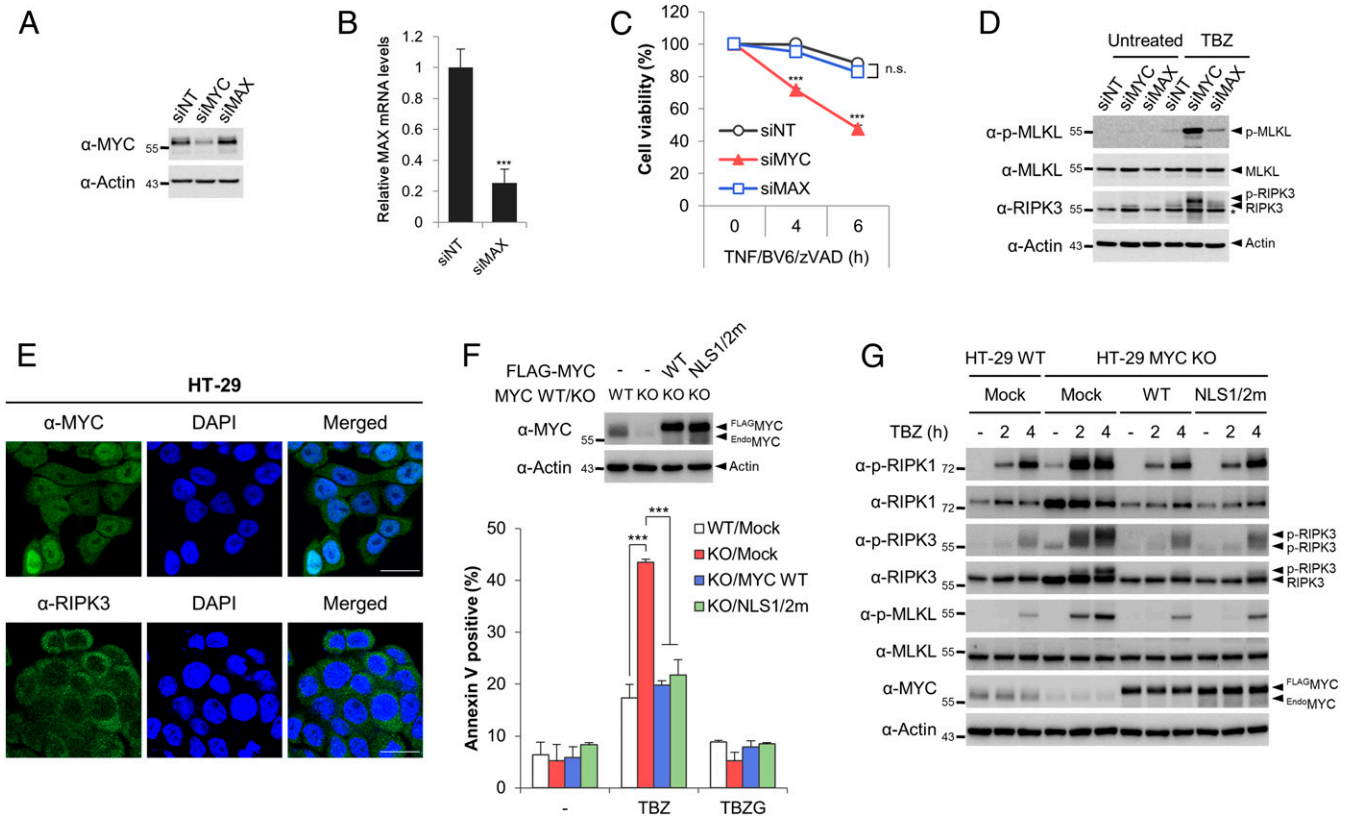

Fig. 4. MYC controls necroptosis in a transcription-independent manner. (*A* and *B*) Immunoblot (*A*) and qRT-PCR (*B*) analyses showing the knockdown efficiency in HT-29 cells. (*C* and *D*) MAX depletion fails to facilitate TNF-α–mediated necroptosis. HT-29 cells transfected with the indicated siRNA pools were treated with TBZ as indicated, followed by cell viability (*C*) and immunoblot (*D*) analyses. Data are the means ± SD, $n = 3$, with $***P < 0.001$, and n.s. = nonsignificant compared to siNT at each point with a two-sided Student's *t* test. The asterisk indicates MLKL. (*E*) Immunofluorescence staining showing the subcellular localization of endogenous MYC and RIPK3 using anti-MYC (#5605, Cell Signaling) and anti-RIPK3 antibodies (#13526, Cell Signaling) in HT-29 cells. (Scale bars, 20 μm.) (*F* and *G*) Both MYC WT and the NLS1/2 mutant (NLS1/2m) suppress the increased necroptosis observed in HT-29/MYC KO cells. HT-29/MYC KO cells reconstituted with lentiviral MYC WT or NLS1/2m cells were treated with TBZ in the absence or presence of GSK'963 (*F*) or with TBZ for the indicated times (*G*). Cell viability (*F*) and immunoblot analyses (*G*) were performed to monitor necroptosis.

from wheat germ cells inhibited the interaction between the RHIM domains of RIPK1 and RIPK3 in vitro (Fig. 6*B*).

We conducted a domain-mapping analysis to identify the domains of MYC essential for suppressing necroptosis and revealed that the N and C termini of RIPK3 and MYC were involved in their interactions, suggesting the presence of multiple binding sites between the two proteins (*SI Appendix*, Fig. S8 *A–D*). Furthermore, the N terminus of MYC (1–144) preferentially interacted with the C terminus of RIPK3 (294–518), while the C terminus of MYC (368–439) bound to the N-terminal kinase domain of RIPK3 (1–293) (*SI Appendix*, Fig. S8*E*). In particular, the N terminus of MYC failed to interact with RIPK3 lacking the RHIM domain (294–454), implying a pivotal role for the RHIM domain in this interaction (*SI Appendix*, Fig. S8*F*). Supporting this hypothesis, the mutation of VQVG, critical residues in the RIPK3 RHIM domain, to AAAA abrogated the interaction of RIPK3 with MYC (*SI Appendix*, Fig. S8 *G* and *H*). Similarly, MYC also interacted with the RHIM domain of RIPK1 (*SI Appendix*, Fig. S8 *I–K*). We tested whether MYC fragments suppressed necroptosis by binding to RIPK3 and RIPK1, and found that both the N and C termini of MYC inhibited TBZ-induced necroptosis (*SI Appendix*, Fig. S8 *L* and *M*). Although the C terminus of MYC bound to the kinase domain of RIPK3 and suppresses necroptosis, MYC did not inhibit the autokinase activity of RIPK3 (*SI Appendix*, Fig. S8*N*). However, the N terminus of MYC (1–144) directly disrupted the formation of the RIPK1–RIPK3 complex in vitro (Fig. 6*C*). Thus, MYC abrogates binding of the RIPK3 RHIM domain to RIPK1, possibly suppressing multimerization and amyloid formation of the necrosome (48, 49).

MYC Depletion Induces the Formation of Sublethal RIPK1–RIPK3 Complexes in a Kinase-Dependent Manner in the Absence of Necroptotic Stimuli. Notably, we consistently observed increased levels of the RIPK3 and RIPK1 proteins in the MYC-depleted and KO cells (Fig. 6 *D* and *E* and *SI Appendix*, Fig. S3*C*). However, the levels of the RIPK1 and RIPK3 mRNAs and levels of the caspase-8, MLKL, cIAP-1/2, and c-FLIP proteins were not affected by changes in the levels of the MYC protein in our system (*SI Appendix*, Figs. S3*C* and S9 *A* and *B*) (50). In contrast, MYC overexpression reduced the levels of the RIPK1 and RIPK3 proteins without significant changes in the mRNA levels (Fig. 1*F* and *SI Appendix*, Fig. S9 *C–E*). In addition, the MYC NLS1/2 mutant, which lacks of transcriptional activity, reduces the levels of the RIPK1 and RIPK3 proteins (Fig. 4*G*), implying that MYC controls the steady-state levels of RIPK1 and RIPK3 in the cytoplasm. As shown in our previous study, RIPK1 and RIPK3 are simultaneously degraded via the CHIP–lysosome-dependent pathway, which suppresses necroptosis (51). Based on these observations, we tested whether MYC-mediated RIPK1 and RIPK3 protein destabilization is also dependent on these systems. Knockdown of MYC, CHIP, or both proteins exerted similar effects on the levels of the RIPK1 and RIPK3 proteins, suggesting that MYC and CHIP may function in the same axis

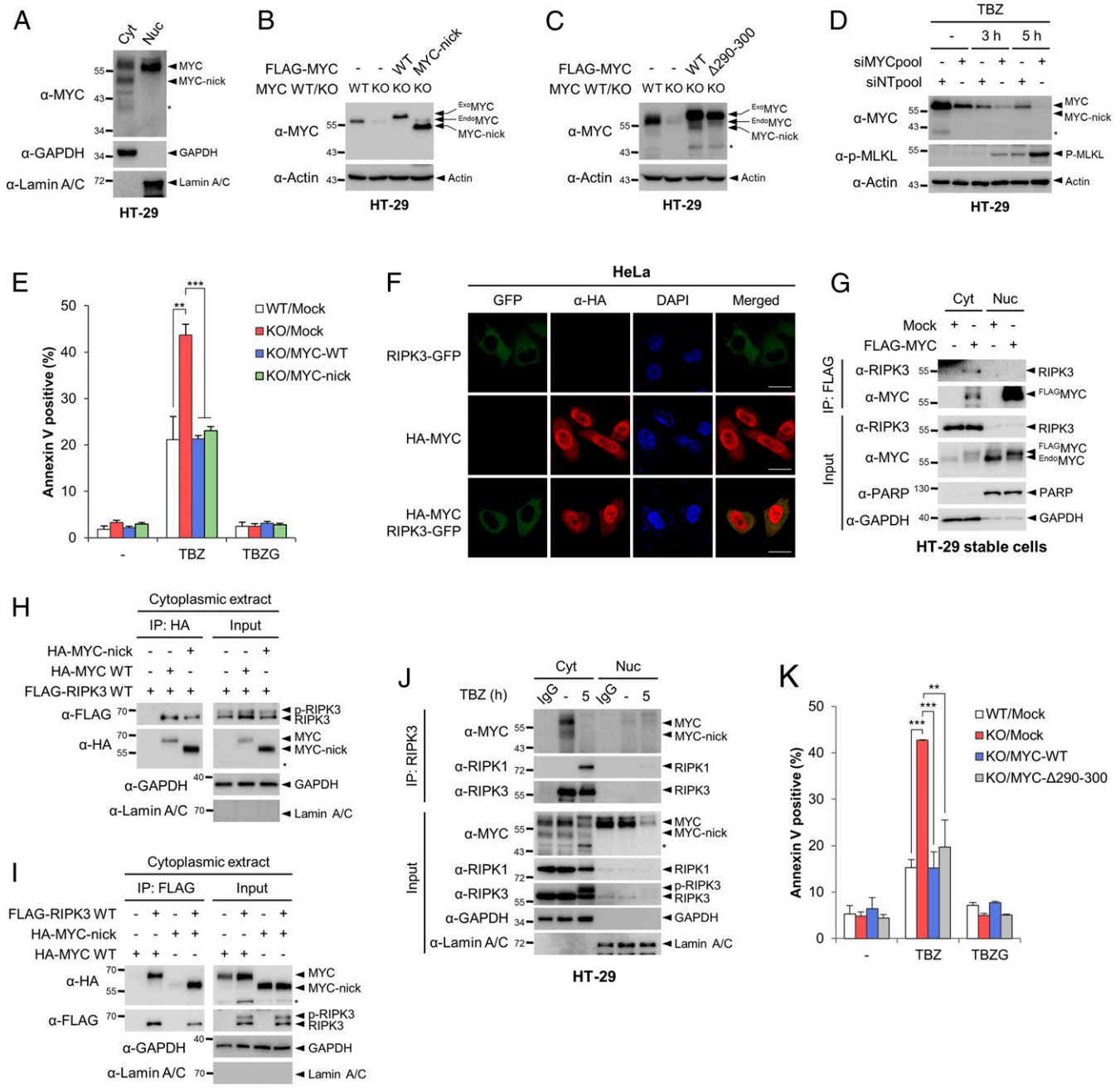

Fig. 5. Both full-length MYC and MYC-nick are responsible for suppressing necroptosis. (*A*) The levels of MYC and MYC-nick in the cytoplasm and nucleus were determined by performing an immunoblot analysis using anti-MYC antibodies (#5605, Cell Signaling). The asterisks indicate a MYC variant. (*B* and *C*) Expression of FLAG-tagged MYC, MYC-nick, and MYC Δ290–300 in HT-29/MYC KO cells. HT-29/MYC KO cells were reconstituted with lentiviral MYC expression vectors, followed by immunoblot analyses. (*D*) Levels of both the MYC and MYC-nick proteins were decreased in response to TBZ stimulation in HT-29 cells. (*E*) Analysis of the viability of HT-29 cells/MYC KO cells reconstituted with MYC and MYC-nick after treatment with TBZ in the absence or presence of GSK′963. Data are the means ± SD, $n = 3$, with $^{**}P < 0.01$ and $^{***}P < 0.001$ compared to MYC KO/Mock cells with a two-sided Student's *t* test. (*F*) Immunofluorescence staining showing cytoplasmic colocalization of HA-MYC and RIPK3-GFP transiently expressed in HeLa cells. (Scale bars, 20 μm.) (*G*) Interaction between endogenous RIPK3 and FLAG-MYC in the cytoplasm. Cytoplasmic and nuclear extracts from HT-29 cells stably expressing FLAG-MYC were immunoprecipitated with anti-FLAG antibodies. FLAG-MYC-bound proteins were isolated using a FLAG peptide to eliminate nonspecific interactions, followed by immunoblotting. (*H* and *I*) Immunoprecipitation analysis using cytoplasmic extracts of 293FT cells transfected with RIPK3 and MYC or MYC-nick (1–298), as indicated. Immunoprecipitates were eluted with the HA or FLAG peptide. (*J*) Endogenous MYC and MYC-nick physiologically associated with endogenous RIPK3 in the cytoplasm. Cytoplasmic and nuclear extracts from HT-29 cells treated with TBZ as indicated were immunoprecipitated using an anti-RIPK3 antibody to examine the endogenous interaction between RIPK3 and MYC. (*K*) Analysis of the viability of the indicated cells after treatment with TBZ. Data are the means ± SD, $n = 3$, with $^{**}P < 0.01$ and $^{***}P < 0.001$ compared to MYC KO/Mock cells with a two-sided Student's *t* test.

(*SI Appendix*, Fig. S9*F*). The destabilization of RIPK1 and RIPK3 by MYC overexpression was blocked by treatment with the lysosome inhibitors E64d and pepstatin A (pepA), but not the proteasome inhibitor MG132 (*SI Appendix*, Fig. S9*G*). Furthermore, MYC-mediated RIPK1 and RIPK3 degradation was completely inhibited by CHIP ablation (*SI Appendix*, Fig. S9*H*).

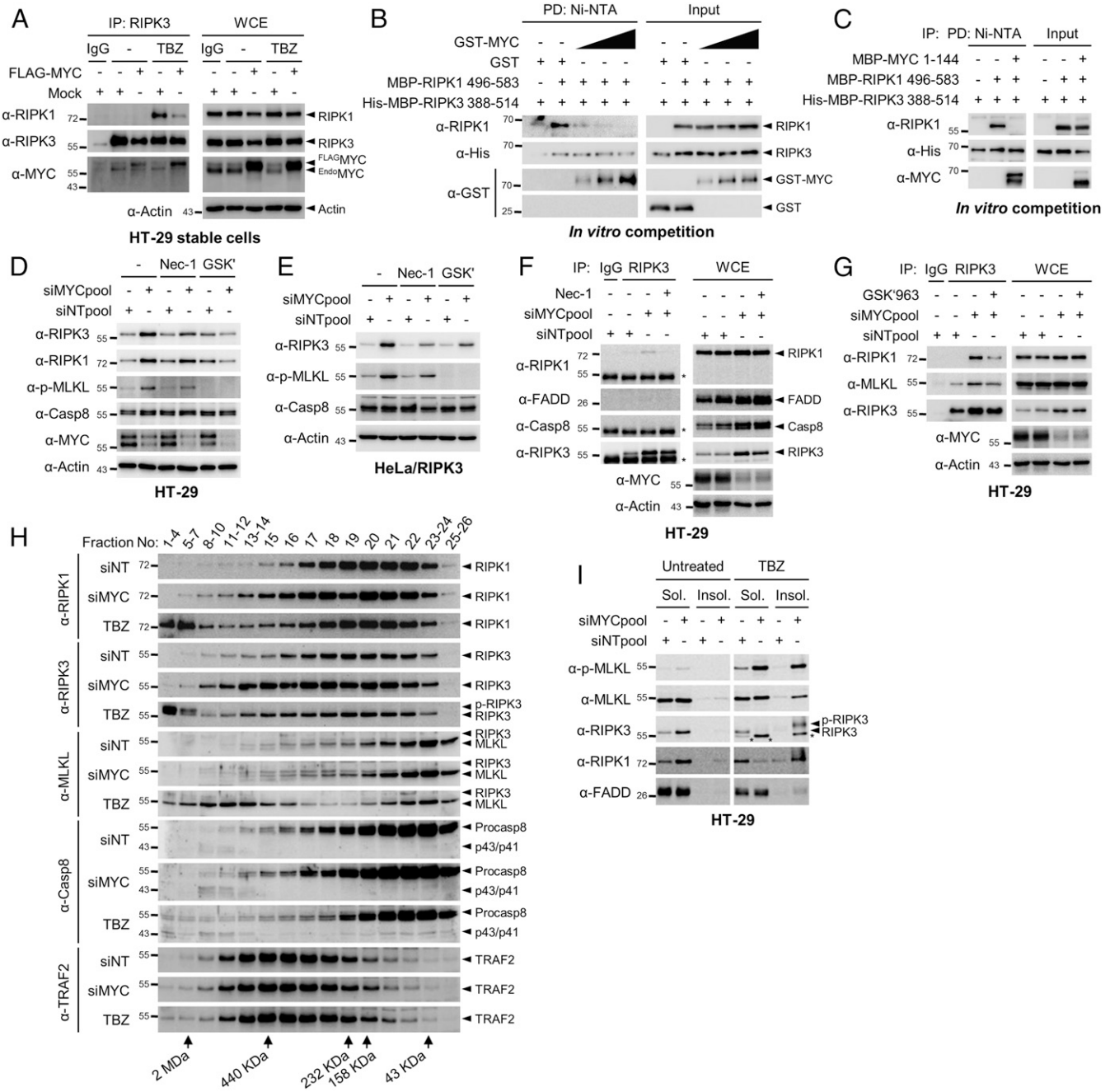

Fig. 6. MYC interacts with RIPK3 and disrupts the interaction between RIPK1 and RIPK3. (*A*) MYC prevents RIPK3 from interacting with RIPK1. HT-29 cells stably expressing FLAG-MYC or empty vector were immunoprecipitated with an anti-RIPK3 antibody. (*B*) MYC prevents the interaction between RIPK1 and RIPK3 in vitro. Recombinant GST-MYC purified using a wheat germ system was added to the recombinant MBP-RIPK1 RHIM domain (496–583) and His-MBP-RIPK3 (388–514) as indicated, followed by Ni^{2+}-pulldown analysis. RIPK3-bound RIPK1 was detected using anti-RIPK1 antibodies. (*C*) The N terminus of MYC is responsible for suppressing the RIPK1 and RIPK3 interaction. Bacterially purified MBP-MYC (1–144) was added to the RHIM domains of RIPK1 and RIPK3. The interaction of RIPK1 and RIPK3 was determined as described above. (*D* and *E*) MYC ablation increases the levels of the RIPK1 and RIPK3 proteins. The levels of the RIPK1, RIPK3, and pMLKL proteins in HT-29 (*D*) and HeLa/RIPK3 cells (*E*) were analyzed using immunoblotting after MYC knockdown and/or treatment with 30 μM Nec-1 or 3 μM GSK′872. (*F* and *G*) RIPK1 and RIPK3 form a complex in MYC-depleted HT-29 cells. HT-29 cells transfected with the indicated siRNAs were treated with DMSO, GSK′963, or Nec-1. After chemical treatment, an immunoprecipitation assay was carried out using an anti-RIPK3 antibody. (*H*) MYC depletion induces the formation of small and inactive necrosome complexes. HT-29 cells were transfected or treated with the indicated siRNA or stimuli, respectively. The cell lysates were fractionated according to molecular size by gel-filtration chromatography and examined by immunoblotting. (*I*) MYC induces the accumulation of RIPK1 and RIPK3 proteins in the soluble fraction. HT-29 cells were transfected with MYC siRNA and treated with TBZ for 4 h. Cells were then fractioned into lysis buffer soluble (Sol.) and insoluble (Insol.) fractions, followed by immunoblot analysis. The phosphorylated form of RIPK3 (p-RIPK3) is indicated by the arrowhead, and the asterisks indicate p-MLKL.

These observations indicated that the MYC-dependent destabilization of RIPK proteins requires the presence of the CHIP–lysosome-dependent pathway.

Because MYC inhibits the interaction between RIPK1 and RIPK3 and MYC ablation increases the RIPK1 and RIPK3 protein levels, we hypothesized that MYC silencing would lead

to sublethal RIPK1–RIPK3 complex formation, which in turn allows these proteins to stabilize themselves but no other related proteins. Indeed, while RIPK3 might rarely interact with RIPK1 under normal conditions, the association between endogenous RIPK1 and RIPK3 was detected in MYC-depleted cells without necroptotic stimulation (Fig. 6 *F* and *G*). Moreover, the association between RIPK3 and MLKL was strengthened by MYC depletion (Fig. 6*G*). These enhanced associations were weakened by GSK′963 or Nec-1, suggesting a requirement for RIPK1 kinase activity (Fig. 6 *F* and *G*). Furthermore, when the MYC-depleted cells were treated with Nec-1 or GSK′872, the accumulation of RIPK3 and phosphorylation of MLKL were suppressed, suggesting the necessity of the kinase activities of RIPK1 and RIPK3 for the stabilization of these proteins (Fig. 6 *D* and *E*). Stabilization of RIPK1 and RIPK3 upon MYC depletion or deletion led to the phosphorylation of RIPK1, RIPK3, and MLKL in the absence of necroptotic stimuli, but the levels of these phosphorylated proteins were much lower than the levels observed during necroptosis (*SI Appendix*, Fig. S9 *I* and *K*). Notably, the phospho-RIPK3 S227 antibody appears to be very specific, as this antibody did not detect the RIPK3 S227A mutant (*SI Appendix*, Fig. S9*J*). As a result, MYC depletion or deletion did not induce MLKL oligomerization and cell death in the absence of necroptotic stimuli (Fig. 2*E* and *SI Appendix*, Fig. S9*K*). Interestingly, the RIPK3 and MLKL phosphorylation observed upon MYC depletion were independent of TNF-α autocrine signaling (*SI Appendix*, Fig. S9 *L* and *M*), suggesting a direct role for MYC in the regulation of necroptosis mediators.

We performed gel-filtration chromatography to further ascertain whether MYC obstructs the formation of the RIPK1–RIPK3 complex in unstimulated cells and found that RIPK1 and RIPK3 were present in the higher molecular mass fractions at ∼300 kDa to 1 MDa in MYC-depleted cells compared to control cells, whereas the distributions of the other proteins, such as caspase-8, MLKL, and TRAF2, remained the same (Fig. 6*H* and *SI Appendix*, Fig. S9*N*). However, RIPK1 and RIPK3 in MYC-depleted cells appeared to form smaller complexes than the typical necrosome, which is larger than 2 MDa (Fig. 6*H*) (29, 39, 40). Notably, RIPK1 and RIPK3 were mainly present in the soluble fraction of MYC-depleted HT-29 cells, but they rapidly shifted to the insoluble fraction in response to necroptotic stimulation (Fig. 6*I*). Our findings revealed that MYC depletion induces the preassembly of small and soluble necrosomes, which are insufficient to trigger necroptosis but may accelerate necroptotic kinesis by facilitating the rapid formation of large and insoluble necrosomes upon necroptotic stimulation.

Suppression of MYC in Leukemia Cells Facilitates Necroptosis-Dependent Cell Death In Vivo and In Vitro. The observation that MYC functions as an antinecroptotic factor suggests the possible therapeutic potential of targeting necroptosis in cancer treatment. We focused on human leukemia cells because frequent overexpression and activation of MYC in human leukemia form the basis of anti-MYC therapy (52, 53). In addition, at very low concentrations, a Smac mimetic resulted in substantially increased sensitivity of several types of leukemia cells to apoptosis and necroptosis through autocrine TNF-α production (Fig. 7*A*) (54–57). We therefore examined the expression of MYC and cell death-related proteins to test the sensitivity to necroptosis of these cells (Fig. 7*B*). Similar to previous observations, cell lines expressing RIPK3, such as Molm13, Molm14, and MV4;11, were sensitive to necroptosis induced by birinapant and zVAD-fmk, but not apoptosis induced by birinapant alone (Fig. 7*C*) (58, 59). HL-60 and CCRF-CEM cells appeared to be sensitive to both apoptosis and necroptosis, whereas NB4 cells lacking RIPK3 were sensitive to apoptosis (Fig. 7*C*). In addition, RS4;11, U937, and KG-1α cells were only resistant to Smac mimetic-induced cell death (Fig. 7*C*). We therefore chose Molm13 cells for further analysis because of their high sensitivity to necroptosis in the absence of TNF-α through autocrine TNF-α production (*SI Appendix*, Fig. S10*A*) (54–57). MYC-depleted Molm13 cells were also more susceptible to necroptosis induced by birinapant and zVAD-fmk (*SI Appendix*, Fig. S10*B*). We also tested another caspase inhibitor, emricasan, which has been examined in clinical trials (54). Again, MYC depletion sensitized cells to necroptosis induced by birinapant and emricasan. Similar to HT-29 cells, MYC depletion leads to an increase in the formation of the necrosome complex and phosphorylation of RIPK3 and MLKL upon necroptotic simulation in Molm13 cells (Fig. 7 *D*–*F* and *SI Appendix*, Fig. S10 *C* and *D*). These results imply that MYC also plays a key role in protecting leukemia cells from necroptosis.

We next conducted a xenograft analysis using MYC-depleted Molm13 cells. Mice with subcutaneous tumors were treated with birinapant and emricasan every 2 d (Fig. 7*G*). Tumors treated with birinapant plus emricasan were slightly smaller than those treated with the vehicle control, consistent with a previous report (Fig. 7 *G*–*J*) (54). Although MYC depletion did not exert a significant effect on tumor growth, it substantially inhibited tumor growth in mice injected with birinapant and emricasan (Fig. 7 *G*–*J*). Strikingly, the tumor mass of MYC-depleted Molm13 cells subjected to the same treatment was significantly reduced, while the tumor mass of cells that did not receive treatment was not. Therefore, although MYC knockdown did not substantially affect tumor growth, it noticeably sensitized the tumor to necroptotic shock (Fig. 7 *G*–*J*). Collectively, the down-regulation of MYC renders leukemia cells more sensitive to necroptosis both in vivo and in vitro, and thus the concept of necroptosis-induced cell death can be applied to cancer therapy.

Discussion

MYC is a versatile and potent oncogene that functions as a master regulator of cancer cells by regulating multiple processes, such as apoptosis, proliferation, stemness, metabolism, and immunity (53, 60–62). While most of these functions are inherently associated with MYC transcriptional activities, here we report an unconventional cytosolic role for MYC as a direct negative regulator of necroptosis wherein MYC functions by interacting with RIPK3, which is a pivotal factor in necroptosis. When the MYC levels were low or ablated, stable RIPK1–RIPK3 complexes with an insufficient capability to induce necroptotic cell death spontaneously formed. Stabilization of RIPK1–RIPK3 complexes relies on phosphorylation because the inhibition of RIPK1 or RIPK3 abolished complex formation and destabilized the RIPK1 and RIPK3 proteins (Fig. 6 *D*–*G*). Upon necroptotic stimulation, these small complexes act as seeding complexes, leading to the rapidly increased formation of active necrosomes, inducing massive necroptotic cell death (63). When MYC is present, MYC directly interacts with RIPK3, thereby preventing the spontaneous formation of the RIPK1 and RIPK3 complexes. This interaction might render CHIP E3 ubiquitin ligase accessible to RIPK1 and RIPK3, leading to their lysosomal degradation, as reported in a previous study (51). Upon necroptotic stimulation, the MYC interaction with RIPK3 delayed the formation of necrosomes, resulting in the suppression of otherwise rapidly occurring necroptosis.

The inhibitory effect of MYC on necroptosis appears to occur in the cytosol because the MYC mutants MYC-nick and NLS1/2m, which are incapable of localizing to the nucleus, suppressed necroptosis (Figs. 4 and 5 and *SI Appendix*, Figs. S5 and S6). Nevertheless, we were unable to exclude a possible nuclear interaction between RIPK3 and MYC, based on a recent report suggesting that the RIPK3 and RIPK1 association in the nucleus might facilitate prenecrosome complex formation, which can accelerate necroptosis (63, 64). After treatment with leptomycin B (LMB), an inhibitor of nuclear export, we observed the accumulation and colocalization of RIPK3 and MYC in the

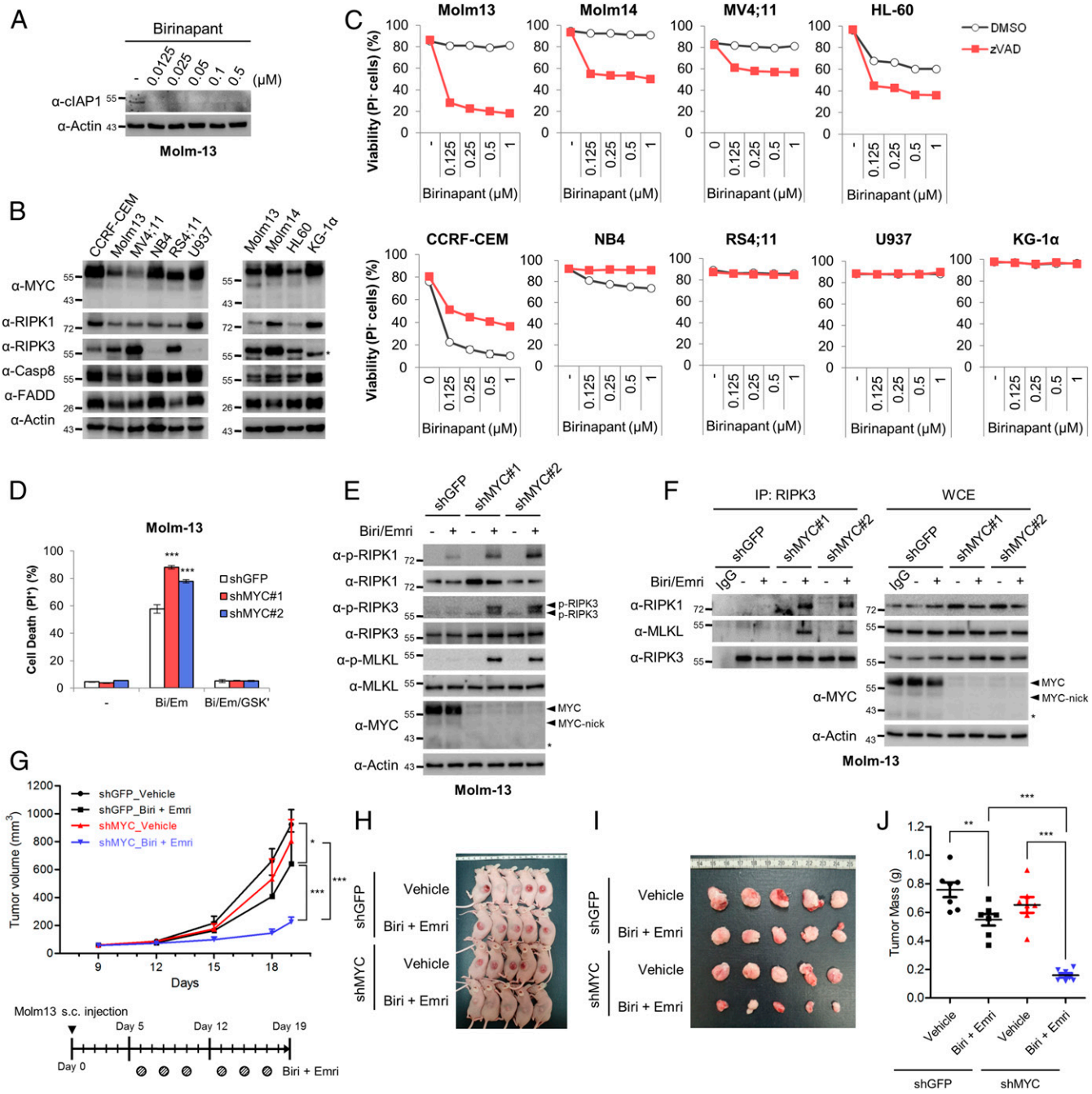

Fig. 7. Down-regulation of MYC sensitizes acute myeloid leukemia cells to necroptosis induced by birinapant plus the caspase inhibitor and increases the antileukemia activity in xenograft models. (*A*) The effects of birinapant (Bi) on the levels of cIAP1 in Molm13 cells. (*B*) Immunoblot analysis of various leukemia cell lines. (*C*) Each leukemia cell line was treated with the indicated concentrations of birinapant alone or birinapant plus 20 μM zVAD for 24 h, followed by a FACS analysis to measure cell viability. (*D–F*) Necroptosis and necrosome analysis of Molm13 cells stably expressing shMYC and treated with 25 nM birinapant plus 1 μM emricasan. GSK′963 (RIPK1 inhibitor) was administered to cells at 100 nM to inhibit RIPK1-dependent necroptosis. After treatment, the cells were examined using a FACS analysis to determine the percentage of cell death (*D*), using an immunoblot analysis to determine the phosphorylation of RIPK3 and MLKL (*E*), and using immunoprecipitation to analyze the necrosome (*F*). (*G–J*) MYC depletion suppresses tumor growth after treatment with birinapant (Bir) and emricasan (Emri) in vivo. A total of 5×10^5 Molm13 cells were implanted subcutaneously into the flank of 6-wk-old nude mice. After 6 d, the mice were treated with Bir (2 mg/kg) plus Emri (1 mg/kg) as indicated by intraperitoneal injection for 2 wk, and tumor growth is shown in *G*. Data are the means ± SEM, $n = 7$ per treatment group, with $^*P < 0.05$ and $^{***}P < 0.001$ at 19 d after the Molm13 cell injection according to a two-tailed Mann–Whitney test. Tumor-bearing mice (*H*), excised tumors (*I*), and tumor masses (*J*) are shown. Data are presented as the mean values and individual data points from $n = 7$ mice, with $^{**}P < 0.01$, $^{***}P < 0.001$, and n.s. = nonsignificant according to the two-tailed Mann–Whitney test.

nucleus in the absence of necroptotic stimuli (*SI Appendix*, Fig. S11 *A* and *B*). While RIPK3 forms large aggregates in the cytoplasm in response to the induction of necroptosis with TBZ, it exhibited nuclear localization and a cytoplasmic small punctate structure upon treatment with TBZ plus LMB (*SI Appendix*, Fig. S11*C*). These data indicate that the interaction between the nuclear shuttling of RIPK3 and MYC also occurs in the nucleus and might suppress necroptosis.

Previously, MYC was shown to sensitize cells to TNF-α– and RIP1-dependent apoptosis in fibroblasts and several types of cancer cells, in part due to the decrease in levels of the $FLIP_L$ protein (37, 38, 50, 65). Moreover, complex IIb formation and subsequent apoptosis in HeLa cells, which lack RIPK3 expression, was slightly suppressed by MYC depletion (Figs. 2*D* and 3*C*) (50, 65). Interestingly, while MYC depletion increased c-$FLIP_L$ expression in several cell lines—including HeLa, HCT116, U2OS, and WI38 cells—it did not affect c-$FLIP_L$ expression in HT-29 and Molm13 cells (*SI Appendix*, Fig. S12). As a result, TNF-α–induced complex IIb formation and apoptosis in HT-29 were not affected by MYC depletion (Figs. 2 *A* and *B* and 3*A*). Based on these observations, the regulation of c-$FLIP_L$ and apoptosis by MYC depends on the context and further studies are needed to address these issues in the future.

Curiously, during necroptosis, RIPK3 activation leads to the proteasomal degradation of MYC and thereby suppresses MYC/MAX-dependent transcriptional programs, indicating a mutual inhibitory effect of RIPK3-mediated necroptosis and MYC. Although the kinase activity of RIPK3 is required for MYC degradation, it is not yet clear whether RIPK3 directly induces MYC degradation (*SI Appendix*, Fig. S2). Given that increase of ubiquitination on MYC during necroptosis, other proteins, such as E3 ubiquitin ligases, might be involved to facilitate MYC degradation when RIPK3 is activated by necroptotic stimuli, which requires further investigation. During necroptosis, RIPK3 phosphorylation by RIPK1 appears to induce MYC release form RIPK3 interaction, followed by MYC degradation (*SI Appendix*, Fig. S7*D*). In this case, the disappearance of MYC might contribute to necroptosis-induced inflammation in the late phase of cell death, as MYC is a well-known antiinflammatory transcription factor (28, 66).

MYC is a master regulator of proliferation and metabolism in cancer, and MYC-dependent modulation of these activities might contribute to regulating necroptosis (62). Indeed, HT-29 cells completely depleted of MYC by the KO system exhibited a slower proliferation rate than the control cells (*SI Appendix*, Fig. S13 *A* and *B*). Nevertheless, transient depletion of MYC for 48 h increased the sensitivity to necroptosis but had little effect on proliferation, cellular ATP levels, and cell death, suggesting that MYC might regulate necroptosis independent of its effects on proliferation and metabolism (Fig. 1 and *SI Appendix*, Fig. S13 *C–E*). While we are unable to exclude the possible effects of the transcriptional activities of MYC on necroptosis, MYC prevented necroptotic cell death through a mechanism independent of its transcriptional activity.

While necroptosis efficiently causes cell death in various types of tissues, it often fails to induce cell death in most tumors due to a lack of RIPK3 expression (25). In contrast, several cancer types, such as leukemia, lymphoma, and colon cancer, contain intact RIPK3 and undergo necroptosis (2, 54, 59, 67). Although the contribution of necroptosis to early tumorigenesis is controversial (68, 69), approaches designed to enhance necroptosis represent a promising therapeutic strategy for established tumors (54–56). The observation that MYC depletion dramatically enhances necroptosis in the presence of birinapant and emricasan in vitro and in vivo indicates that MYC might have been evolutionarily selected by tumor cells to suppress necroptosis. As MYC negatively regulates RIPK3, modulation of this pathway may be a therapeutic strategy for treating cancer or inflammatory diseases.

Materials and Methods

Cell Viability Analysis and Flow Cytometry. For the analysis of cell viability, cells were incubated with the CellTiter-Glo reagent and analyzed with a luminometer according to the manufacturer's protocol (CellTiter-Glo Luminescent Cell Viability Assay kit, G7571, Promega). For Annexin V and 7-AAD double staining, prepared cells were harvested and washed with PBS, followed by incubation with Annexin V-FITC (556547; BD Biosciences) and 7-AAD (00-6993-50, eBioscience) in Annexin V Binding Buffer (51-66121E, BD Biosciences) for 15 min according to the manufacturer's protocol. For propidium iodide (PI) single staining, each leukemia cell line was harvested and washed with PBS, followed by an incubation with PI for 15 min. Dead cells were determined as the PI^+ population, and viable cells were determined as the PI^- population by flow cytometry (BD Accrui C6, BD Biosciences). Data were analyzed using BD Accuri C6 Plus software (BD Biosciences).

Immunofluorescence Analysis. HT-29 cells were plated on confocal dishes (100350, SPL). After treatment with the indicated chemicals, the cells were fixed with 4% paraformaldehyde for 10 min at room temperature. Cells were incubated with immunofluorescence blocking buffer (PBS with 3% BSA, 1% saponin, and 1% Triton X-100) containing anti-MYC (1:100; 5605, Cell Signaling) or anti-RIPK3 antibodies (1:50; 13526. Cell Signaling) overnight at 4 °C. Samples were washed with PBS three times and then incubated with Alexa Fluor 488 anti-rabbit (1:200; A-11008, Thermo Fisher Scientific) supplemented in immunofluorescence blocking buffer for 1 h. HeLa cells were cultured on confocal dishes (100350, SPL). Cells were transfected with HA-MYC- and RIPK3-GFP-expressing plasmids and then treated with the indicated chemicals. After treatments, the cells were fixed with 4% paraformaldehyde for 10 min at room temperature and then permeabilized via incubation with PBS containing 0.1% Triton-X 100. The samples were incubated with PBS containing 2.5% BSA and anti-HA antibody (1:100; sc-7392, Santa Cruz Biotechnology) for 2 h. The cells were washed with PBS three times and then incubated with Alexa Fluor 594 anti-mouse (1:200; A-11005, Thermo Fisher Scientific) for 1 h. DAPI was used to stain the nuclei. All stained samples were analyzed with a confocal microscope (LSM 800, Carl Zeiss).

Gel-Filtration Chromatography Analysis. HT-29 cells were transfected with a nontargeting siRNA pool (siNT) and MYC siRNA pool (siMYC) for 48 h and then treated with 20 ng/mL TNF-α, 2 μM BV6, and 30 μM zVAD-fmk for the indicated times. Cells were collected from the seven 100-mm culture dishes and lysed with 2.5 mL of lysis buffer containing 50 mM Tris·HCl (pH 7.5), 150 mM NaCl, 0.5% Triton X-100, and 1 mM EDTA, and lysates were injected in an AKTA Prime Plus system and separated on a HiLoad 16/600 Superdex 200 column at a flow rate of 0.4 mL/min (GE Healthcare). Fractions of 2 mL were collected, and samples were analyzed using Western blotting with the indicated antibodies. Molecular weight markers were determined by gel-filtration calibration kits (GE Healthcare).

MLKL Oligomerization. Cells were directly lysed in nonreducing 2× sample buffer containing 100 nM Tris·HCl, 4% SDS, 20% glycerol, 20 mM EDTA, and bromophenol blue without β-mercaptoethanol. For reducing conditions, 200 mM β-mercaptoethanol was added to nonreducing lysates. Both nonreducing and reducing lysates were boiled for 10 min.

Xenograft Study. The subcutaneous tumor xenograft model was established by resuspending ~5×10^5 Molm13 cells expressing shRNAs in 50 μL of PBS and 50 μL of Matrigel matrix (354234, BD Sciences) and subcutaneously inoculating the mixture into the flank of 6-wk-old female BALB/c nude mice (Narabiotech). Six days after inoculation, the mice bearing xenograft tumors were intraperitoneally injected with birinapant (2 mg/kg) plus emricasan (1 mg/kg), as indicated in Fig. 7*G*. Nineteen days after inoculation, the mice were killed and the tumor volumes and masses were measured using a previously described method (70). All animal experiments related to the subcutaneous tumor xenograft model were approved by the Institutional Animal Care and Use Committee of the Laboratory Animal Research at Yonsei University (IACUC-A-201703-174-02).

Data Availability. Major protocols, cell viability analysis and flow cytometry, immunofluorescence analysis, gel-filtration chromatography analysis, MLKL oligomerization, and xenograft study are described in *Materials and Methods*. See *SI Appendix, SI Materials and Methods* for a detailed description of cell culture, plasmids and transfection, generation and validation of the MYC KO cell lines, information of siRNA, shRNA, chemicals, and cell death stimulation, immunoprecipitation and immunoblotting, cytoplasmic/nuclear and soluble/insoluble fractionation, protein purification, in vitro binding and kinase assays, qRT-PCR, RNA sequencing and GSEA, and statistics. RNA sequencing data have been deposited in the Gene Expression Omnibus database (accession no. GSE121149).

ACKNOWLEDGMENTS. This study was supported by a grant from the National Research Foundation of Korea (NRF) funded by the Ministry of Science, ICT and Future Planning (NRF-2015R1A3A2066581) and Brain Korea 21 (BK21) PLUS

program (both to J. Song); a grant from the Basic Science Research Program through the NRF funded by the Ministry of Education (NRF-2019R1C1C1002831); a grant from the Korea Research Institute of Bioscience and Biotechnology Research Initiative Program (to E.-W.L.); a grant from Graduate School of Yonsei University Research Scholarship Grants in 2020 (to D.S.); and grants from the National Cancer Center (1710080) and the NRF (NRF-2017M3A9F9030648) (both to D.H.S). Research in the P.V. group is supported by Flemish grants (EOS MODEL-IDI consortium, G.0C31.14N, G.0C37.14N, G.0E04.16N, G.0C76.18N, and G.0B71.18N), Methusalem (BOF16/MET_V/007), 'Foundation against Cancer' (FAF-F/2016/865), and the Vlaams Instituut voor Biotechnologie.

1. Y. S. Cho *et al*., Phosphorylation-driven assembly of the RIP1-RIP3 complex regulates programmed necrosis and virus-induced inflammation. *Cell* **137**, 1112–1123 (2009).
2. S. He *et al*., Receptor interacting protein kinase-3 determines cellular necrotic response to TNF-alpha. *Cell* **137**, 1100–1111 (2009).
3. P. Vandenabeele, L. Galluzzi, T. Vanden Berghe, G. Kroemer, Molecular mechanisms of necroptosis: An ordered cellular explosion. *Nat. Rev. Mol. Cell Biol.* **11**, 700–714 (2010).
4. L. Galluzzi *et al*., Molecular mechanisms of cell death: Recommendations of the Nomenclature Committee on Cell Death 2018. *Cell Death Differ.* **25**, 486–541 (2018).
5. L. Sun *et al*., Mixed lineage kinase domain-like protein mediates necrosis signaling downstream of RIP3 kinase. *Cell* **148**, 213–227 (2012).
6. J. Zhao *et al*., Mixed lineage kinase domain-like is a key receptor interacting protein 3 downstream component of TNF-induced necrosis. *Proc. Natl. Acad. Sci. U.S.A.* **109**, 5322–5327 (2012).
7. T. Delanghe, Y. Dondelinger, M. J. M. Bertrand, RIPK1 kinase-dependent death: A symphony of phosphorylation events. *Trends Cell Biol.* **30**, 189–200 (2020).
8. H. Wang *et al*., Mixed lineage kinase domain-like protein MLKL causes necrotic membrane disruption upon phosphorylation by RIP3. *Mol. Cell* **54**, 133–146 (2014).
9. Y. Dondelinger *et al*., MLKL compromises plasma membrane integrity by binding to phosphatidylinositol phosphates. *Cell Rep.* **7**, 971–981 (2014).
10. Z. Cai *et al*., Plasma membrane translocation of trimerized MLKL protein is required for TNF-induced necroptosis. *Nat. Cell Biol.* **16**, 55–65 (2014).
11. X. Chen *et al*., Translocation of mixed lineage kinase domain-like protein to plasma membrane leads to necrotic cell death. *Cell Res.* **24**, 105–121 (2014).
12. G. Quarato *et al*., Sequential engagement of distinct MLKL phosphatidylinositol-binding sites executes necroptosis. *Mol. Cell* **61**, 589–601 (2016).
13. S. Jouan-Lanhouet *et al*., Necroptosis, in vivo detection in experimental disease models. *Semin. Cell Dev. Biol.* **35**, 2–13 (2014).
14. J. Seo *et al*., The roles of ubiquitination in extrinsic cell death pathways and its implications for therapeutics. *Biochem. Pharmacol.* **162**, 21–40 (2019).
15. X. Qin, D. Ma, Y. X. Tan, H. Y. Wang, Z. Cai, The role of necroptosis in cancer: A double-edged sword? *Biochim. Biophys. Acta Rev. Cancer* **1871**, 259–266 (2019).
16. B. Shan, H. Pan, A. Najafov, J. Yuan, Necroptosis in development and diseases. *Genes Dev.* **32**, 327–340 (2018).
17. D. R. Green, The coming decade of cell death research: Five riddles. *Cell* **177**, 1094–1107 (2019).
18. A. Degterev, D. Ofengeim, J. Yuan, Targeting RIPK1 for the treatment of human diseases. *Proc. Natl. Acad. Sci. U.S.A.* **116**, 9714–9722 (2019).
19. A. J. Legrand, M. Konstantinou, E. F. Goode, P. Meier, The diversification of cell death and immunity: Memento Mori. *Mol. Cell* **76**, 232–242 (2019).
20. Y. Gong *et al*., The role of necroptosis in cancer biology and therapy. *Mol. Cancer* **18**, 100 (2019).
21. S. Philipp, J. Sosna, D. Adam, Cancer and necroptosis: Friend or foe? *Cell. Mol. Life Sci.* **73**, 2183–2193 (2016).
22. S. Fulda, Therapeutic exploitation of necroptosis for cancer therapy. *Semin. Cell Dev. Biol.* **35**, 51–56 (2014).
23. J. R. Cerhan *et al*., Genetic variation in 1253 immune and inflammation genes and risk of non-Hodgkin lymphoma. *Blood* **110**, 4455–4463 (2007).
24. A. L. Nugues *et al*., RIP3 is downregulated in human myeloid leukemia cells and modulates apoptosis and caspase-mediated p65/RelA cleavage. *Cell Death Dis.* **5**, e1384 (2014).
25. G. B. Koo *et al*., Methylation-dependent loss of RIP3 expression in cancer represses programmed necrosis in response to chemotherapeutics. *Cell Res.* **25**, 707–725 (2015).
26. M. D. Cole, The myc oncogene: Its role in transformation and differentiation. *Annu. Rev. Genet.* **20**, 361–384 (1986).
27. M. Conacci-Sorrell, L. McFerrin, R. N. Eisenman, An overview of MYC and its interactome. *Cold Spring Harb. Perspect. Med.* **4**, a014357 (2014).
28. N. Meyer, L. Z. Penn, Reflecting on 25 years with MYC. *Nat. Rev. Cancer* **8**, 976–990 (2008).
29. M. C. de Almagro *et al*., Coordinated ubiquitination and phosphorylation of RIP1 regulates necroptotic cell death. *Cell Death Differ.* **24**, 26–37 (2017).
30. M. C. de Almagro, T. Goncharov, K. Newton, D. Vucic, Cellular IAP proteins and LUBAC differentially regulate necrosome-associated RIP1 ubiquitination. *Cell Death Dis.* **6**, e1800 (2015).
31. N. Yatim *et al*., RIPK1 and NF-κB signaling in dying cells determines cross-priming of $CD8^+$ T cells. *Science* **350**, 328–334 (2015).
32. M. Najjar *et al*., RIPK1 and RIPK3 kinases promote cell-death-independent inflammation by Toll-like receptor 4. *Immunity* **45**, 46–59 (2016).
33. K. Zhu *et al*., Necroptosis promotes cell-autonomous activation of proinflammatory cytokine gene expression. *Cell Death Dis.* **9**, 500 (2018).
34. A. Kaczmarek, P. Vandenabeele, D. V. Krysko, Necroptosis: The release of damage-associated molecular patterns and its physiological relevance. *Immunity* **38**, 209–223 (2013).
35. B. Laukens *et al*., Smac mimetic bypasses apoptosis resistance in FADD- or caspase-8-deficient cells by priming for tumor necrosis factor α-induced necroptosis. *Neoplasia* **13**, 971–979 (2011).
36. M. Ali, E. S. Mocarski, Proteasome inhibition blocks necroptosis by attenuating death complex aggregation. *Cell Death Dis.* **9**, 346 (2018).
37. J. Klefstrom, E. W. Verschuren, G. Evan, c-Myc augments the apoptotic activity of cytosolic death receptor signaling proteins by engaging the mitochondrial apoptotic pathway. *J. Biol. Chem.* **277**, 43224–43232 (2002).
38. J. Klefstrom *et al*., Induction of TNF-sensitive cellular phenotype by c-Myc involves p53 and impaired NF-kappaB activation. *EMBO J.* **16**, 7382–7392 (1997).
39. T. Tenev *et al*., The Ripoptosome, a signaling platform that assembles in response to genotoxic stress and loss of IAPs. *Mol. Cell* **43**, 432–448 (2011).
40. M. Feoktistova *et al*., cIAPs block Ripoptosome formation, a RIP1/caspase-8 containing intracellular cell death complex differentially regulated by cFLIP isoforms. *Mol. Cell* **43**, 449–463 (2011).
41. G. J. Kato, C. V. Dang, Function of the c-Myc oncoprotein. *FASEB J.* **6**, 3065–3072 (1992).
42. A. Cascón, M. Robledo, MAX and MYC: A heritable breakup. *Cancer Res.* **72**, 3119–3124 (2012).
43. C. V. Dang, W. M. Lee, Identification of the human c-myc protein nuclear translocation signal. *Mol. Cell. Biol.* **8**, 4048–4054 (1988).
44. J. Niklinski *et al*., Disruption of Myc-tubulin interaction by hyperphosphorylation of c-Myc during mitosis or by constitutive hyperphosphorylation of mutant c-Myc in Burkitt's lymphoma. *Mol. Cell. Biol.* **20**, 5276–5284 (2000).
45. R. W. Craig, H. L. Buchan, C. I. Civin, M. B. Kastan, Altered cytoplasmic/nuclear distribution of the c-myc protein in differentiating ML-1 human myeloid leukemia cells. *Cell Growth Differ.* **4**, 349–357 (1993).
46. M. Conacci-Sorrell, C. Ngouenet, R. N. Eisenman, Myc-nick: A cytoplasmic cleavage product of Myc that promotes alpha-tubulin acetylation and cell differentiation. *Cell* **142**, 480–493 (2010).
47. M. Conacci-Sorrell, C. Ngouenet, S. Anderson, T. Brabletz, R. N. Eisenman, Stress-induced cleavage of Myc promotes cancer cell survival. *Genes Dev.* **28**, 689–707 (2014).
48. J. Li *et al*., The RIP1/RIP3 necrosome forms a functional amyloid signaling complex required for programmed necrosis. *Cell* **150**, 339–350 (2012).
49. M. Mompeán *et al*., The structure of the necrosome RIPK1-RIPK3 core, a human hetero-amyloid signaling complex. *Cell* **173**, 1244–1253.e10 (2018).
50. H. Wang *et al*., PELI1 functions as a dual modulator of necroptosis and apoptosis by regulating ubiquitination of RIPK1 and mRNA levels of c-FLIP. *Proc. Natl. Acad. Sci. U.S.A.* **114**, 11944–11949 (2017).
51. J. Seo *et al*., CHIP controls necroptosis through ubiquitylation- and lysosome-dependent degradation of RIPK3. *Nat. Cell Biol.* **18**, 291–302 (2016).
52. M. D. Delgado, M. Albajar, M. T. Gomez-Casares, A. Batlle, J. León, MYC oncogene in myeloid neoplasias. *Clin. Transl. Oncol.* **15**, 87–94 (2013).
53. S. A. Abraham *et al*., Dual targeting of p53 and c-MYC selectively eliminates leukaemic stem cells. *Nature* **534**, 341–346 (2016).
54. G. Brumatti *et al*., The caspase-8 inhibitor emricasan combines with the SMAC mimetic birinapant to induce necroptosis and treat acute myeloid leukemia. *Sci. Transl. Med.* **8**, 339ra69 (2016).
55. N. Lalaoui *et al*., Targeting p38 or MK2 enhances the anti-leukemic activity of smac-mimetics. *Cancer Cell* **29**, 145–158 (2016).
56. S. McComb *et al*., Activation of concurrent apoptosis and necroptosis by SMAC mimetics for the treatment of refractory and relapsed ALL. *Sci. Transl. Med.* **8**, 339ra70 (2016).
57. S. L. Petersen *et al*., Autocrine TNFalpha signaling renders human cancer cells susceptible to Smac-mimetic-induced apoptosis. *Cancer Cell* **12**, 445–456 (2007).
58. L. Steinhart, K. Belz, S. Fulda, Smac mimetic and demethylating agents synergistically trigger cell death in acute myeloid leukemia cells and overcome apoptosis resistance by inducing necroptosis. *Cell Death Dis.* **4**, e802 (2013).
59. C. Safferthal, K. Rohde, S. Fulda, Therapeutic targeting of necroptosis by Smac mimetic bypasses apoptosis resistance in acute myeloid leukemia cells. *Oncogene* **36**, 1487–1502 (2017).
60. K. A. Sarosiek *et al*., Developmental regulation of mitochondrial apoptosis by c-Myc governs age- and tissue-specific sensitivity to cancer therapeutics. *Cancer Cell* **31**, 142–156 (2017).
61. K. M. Lee *et al*., MYC and MCL1 cooperatively promote chemotherapy-resistant breast cancer stem cells via regulation of mitochondrial oxidative phosphorylation. *Cell Metab.* **26**, 633–647.e7 (2017).
62. Z. E. Stine, Z. E. Walton, B. J. Altman, A. L. Hsieh, C. V. Dang, MYC, metabolism, and cancer. *Cancer Discov.* **5**, 1024–1039 (2015).
63. K. Weber, R. Roelandt, I. Bruggeman, Y. Estornes, P. Vandenabeele, Nuclear RIPK3 and MLKL contribute to cytosolic necrosome formation and necroptosis. *Commun. Biol.* **1**, 6 (2018).
64. S. Yoon, K. Bogdanov, A. Kovalenko, D. Wallach, Necroptosis is preceded by nuclear translocation of the signaling proteins that induce it. *Cell Death Differ.* **23**, 253–260 (2016).
65. M. S. Ricci *et al*., Direct repression of FLIP expression by c-myc is a major determinant of TRAIL sensitivity. *Mol. Cell. Biol.* **24**, 8541–8555 (2004).
66. S. C. Casey *et al*., MYC regulates the antitumor immune response through CD47 and PD-L1. *Science* **352**, 227–231 (2016).
67. K. Moriwaki, J. Bertin, P. J. Gough, G. M. Orlowski, F. K. Chan, Differential roles of RIPK1 and RIPK3 in TNF-induced necroptosis and chemotherapeutic agent-induced cell death. *Cell Death Dis.* **6**, e1636 (2015).
68. U. Höckendorf *et al*., RIPK3 restricts myeloid leukemogenesis by promoting cell death and differentiation of leukemia initiating cells. *Cancer Cell* **30**, 75–91 (2016).
69. L. Seifert *et al*., The necrosome promotes pancreatic oncogenesis via CXCL1 and Mincle-induced immune suppression. *Nature* **532**, 245–249 (2016).
70. M. Jeong *et al*., USP8 suppresses death receptor-mediated apoptosis by enhancing $FLIP_L$ stability. *Oncogene* **36**, 458–470 (2017).